Hindawi
Structural Control and Health Monitoring
Volume 2024, Article ID 5570667, 17 pages
https://doi.org/10.1155/2024/5570667

Research Article

A Bayesian Structural Modal Updating Method Based on Sparse Grid and Ensemble Kalman Filter

Guangwei Lin,[1] Yi Zhang,[1] Enjian Cai,[1] Min Luo,[2] and Jing Guo[3]

[1]*Department of Civil Engineering, Tsinghua University, Beijing, China*
[2]*Ocean College, Zhejiang University, Hangzhou, Zhejiang, China*
[3]*Marine Environmental Monitoring and Forecasting Center of Zhejiang Province, Hangzhou, Zhejiang, China*

Correspondence should be addressed to Yi Zhang; zhang-yi@tsinghua.edu.cn

Received 8 December 2023; Revised 19 February 2024; Accepted 18 March 2024; Published 8 April 2024

Academic Editor: Zili Zhang

This study presents a sparse grid interpolation and ensemble Kalman filter (EnKF)-based Markov Chain Monte Carlo (MCMC) method (SG-EnMCMC). Initiating with the formulation of a recursive equation for the state space vector, derived from the structural dynamic equation, this study adopts a dimensionality reduction strategy. This approach involves a separation of physical parameters and the state space vector. The acquisition of physical parameters is accomplished through sampling, utilizing sample moments to substitute population moments, thereby mitigating the need for computationally high-dimensional covariance matrix calculations. To further streamline the recursive equation of the state space vector, a sparse grid method is employed for interpolation. This step simplifies the process while ensuring superior accuracy compared to the Extended Kalman Filter (EKF) and Unscented Kalman Filter (UKF). Subsequent to this, acceptance rates and the final parameter posterior distribution within the MCMC framework are derived. The efficiency of the proposed method is assessed through validation in two shaking table experiments.

1. Introduction

Civil engineering structures and infrastructures represent intricate and vital structural systems that exert a significant influence on economic, commercial, and social aspects of life [1, 2]. With the continuous advancements in civil engineering technology, the architectural design objectives have gradually shifted towards achieving high reliability, low cost, and extended service life. To address stress-related issues and mitigate the risk of disasters in complex structures, physical models and simulation models have been widely employed. However, during the operational lifespan of a building structure, it encounters various stimuli, including earthquakes, strong winds, traffic, human activities, and other external forces. Consequently, the structure's performance may fail to meet anticipated requirements, leading to a phenomenon known as structural performance degradation over time [3, 4] and potentially resulting in severe damage, catastrophic failure, and collapse [5, 6].

Furthermore, the reliability of structural analysis is significantly affected by the complex variations in structural strength and loads induced by these stimuli. Numerous uncertain factors contribute to these uncertainties, including epistemic uncertainty and aleatoric uncertainty [7]. Epistemic uncertainty refers to the uncertainty associated with theoretical models. This uncertainty arises from approximations and assumptions made in the physical model used to characterize the structural system [8]. It also stems from the idealization of material properties, connection forms, boundary conditions, and external effects in simulation models. Moreover, construction errors occurring during the construction process and the weakening of component strength due to aging further challenge the accurate representation of the real structure within the theoretical model. Aleatoric uncertainty relates to uncertainties in measured data [9]. Despite the advancements in measurement technology, accurately capturing the structural response for vibration measurement and modal analysis of engineering

structures remains challenging [10]. This difficulty is particularly pronounced for complex and large structures, where effectively obtaining modal parameters remains a significant obstacle. Moreover, the test data are susceptible to noise pollution during the collection, transmission, and storage processes due to the influence of changing environmental conditions and other factors [11]. In general, uncertainties stemming from cognitive and accidental factors play substantial roles in shaping the reliability of structural analysis, given their impact on theoretical models and measured data, respectively.

Therefore, on the basis of considering the uncertainties, the process of updating the physical or simulation model of a structure emerges as a crucial issue and technical challenge within the field of structural dynamics analysis in civil engineering [12–14]. Model updating serves as a structural health monitoring (SHM) approach, wherein modal parameters are identified and updated [15, 16] using vibration signals measured during structural tests. This process involves adjusting and optimizing the physical or simulation model to ensure that the calculated response values of the updated model align with the actual response values obtained experimentally. By employing model updating techniques, the objective is to enhance the accuracy and reliability of the model, thereby ensuring that the structural performance meets the desired requirements.

Model updating has become one of the most challenging problems of structural safety control [17–19]. Conducting research on structural model updating methods holds significant theoretical importance and practical meaning. However, traditional model updating approaches primarily employ deterministic methods, assuming that both measured data and the physical or simulation model are deterministic [20–22]. These methods often overlook the uncertainties discussed earlier and estimate the physical parameters of the model through nonprobabilistic means, disregarding their random characteristics. Consequently, the analysis results typically only reflect the short-term structural condition.

To address this limitation, the focus of model updating research has shifted towards uncertainty updating. Uncertainty is updated using probabilistic approaches, considering the measured data and finite element calculation results as random variables. Bayesian model updating has emerged as one of the most popular techniques employed across various fields [18, 23–25] due to its ability to incorporate prior information while analyzing uncertainties. By adopting Bayesian methods, the advantages of prior knowledge can be effectively utilized, leading to improved uncertainty characterization in structural model updating.

Bayesian model updating approach offers a coherent and rigorous probabilistic framework for systematically characterizing and quantifying uncertainties arising from material properties and modeling errors for a robust structural prediction [4, 26–28]. In the framework of Bayesian model updating approach, the identification of structural model parameters is viewed from the perspective of probability statistics as a problem of solving the optimal model under the quantitative influence of model errors and measurement noises [29]. Afterwards, the structural model is updated to better describe the structural properties and facilitate effective decisions by taking into account dynamic response measurements [30, 31]. The Bayesian model parameter identification method was first proposed by Collins et al. [32]. Beck and Katafygiotis [27] built a more comprehensive and rigorous framework for Bayesian model updating and defined the concept of system identifications. Recently, numerous studies of Bayesian model updating have been developed on analyzing both numerical examples and real-world applications [33–35]. The schematic diagram of Bayesian model updating is shown in Figure 1.

In the context of Bayesian model updating, a critical challenge lies in constructing the likelihood function. As models are often presented in numerical form rather than functional form, establishing a direct connection between physical parameters and the output variables of structural measurements (referred to as structural features below) can be difficult. The Kalman filter (KF) is one of the most widely used methods [36–38]. Developed from Bayesian filtering, the Kalman filter recursively identifies state space parameters of linear systems, updates the parameters using measured values, and obtains the likelihood function to achieve optimal estimation (filtering). However, most structural parameters and responses targeted for modification are nonlinear, whereas the standard Kalman filter equation is only applicable to linear systems [39]. To overcome this limitation, an extension known as the Extended Kalman Filter (EKF) [40] is proposed, considering the advantages of Kalman Filtering (KF) in the context of recursive Bayesian estimation. The EKF is combined with local linearization techniques within the KF framework. However, it is worth noting that for strong nonlinear systems, EKF can be susceptible to filter divergence, primarily due to the cumulative impact of rounding errors [41]. To address the limitations associated with strong nonlinearity, various nonlinear filtering methods have been developed, eliminating the need for the computation of Jacobian matrices. Examples of such methods include the Unscented Kalman Filter (UKF) [42], the Central Difference Filter (CDF) [43], and the Cubature Kalman Filter (CKF) [44]. Nevertheless, these methods exhibit reduced convergence when dealing with systems characterized by pronounced nonlinear and non-Gaussian characteristics. With the advancement of computer capabilities, the Particle Filter (PF), constructed by combining the Sequential Monte Carlo simulation method (SMC) and recursive Bayesian concepts, has garnered increased attention [45, 46]. The PF methodology involves two fundamental steps: prediction and update. In contrast to the KF, which employs sequential importance sampling in the prediction step and resampling in the update step, the PF demonstrates superior filtering accuracy compared to existing nonlinear filtering algorithms such as EKF and UKF. Additionally, EKF and UKF require Gaussian distribution noise, while PF is more flexible and can accommodate non-Gaussian noise distributions [47]. However, PF is challenged by inherent issues related to particle degradation and diminishing particle diversity. Additionally, the accuracy of PF filtering is contingent on the system state dimension and the number of

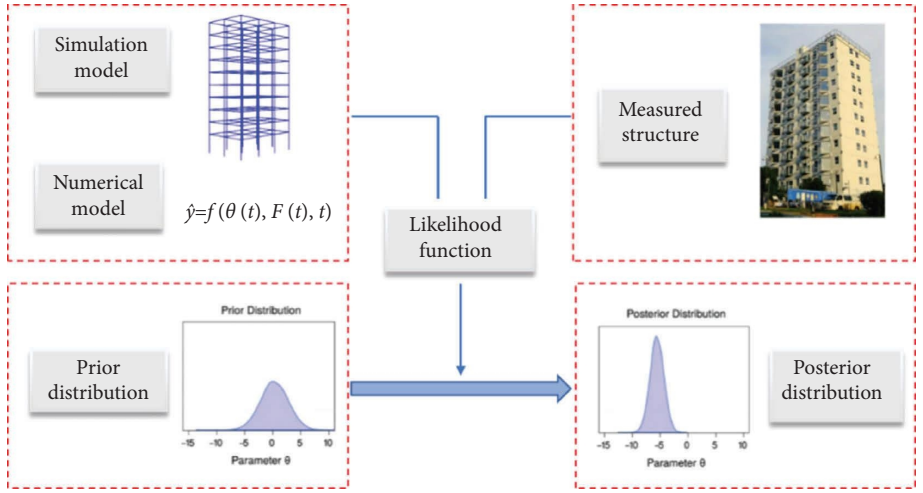

Figure 1: Schematic diagram of Bayesian model updating.

particles, making its parameter settings less universal for diverse applications. In addition to PF, EnKF (Ensemble Kalman Filter), proposed by Evensen [48], combines recursive Bayesian principles with ensemble prediction concepts. EnKF utilizes the SMC method to generate an initial sample set representing the state statistics. It then applies the system state transition function to each sample within the initial set [49]. The current state estimate is subsequently computed by evaluating the mean value and covariance of the sample set after the state transition. Data assimilation techniques are incorporated in EnKF implementation, mitigating the adverse impact of measurement noise randomness on filtering accuracy. EnKF extends the Kalman filtering method to address challenges associated with non-Gaussian and nonlinear dynamics that are difficult to linearize. This method has been developed for geophysical applications and has demonstrated robustness in scenarios characterized by substantial modeling and measurement errors [50]. EnKF is particularly notable for its computational efficiency, surpassing PF in this regard [51].

Despite the significant progress made by scholars in the related fields mentioned above, several challenges persist. In the traditional methods regarding KF, uncertain structural parameters are typically incorporated into the state space vector. Therefore, the sizes of both the state space vector and the state space equation become considerably large. Additionally, the state equation tends to exhibit high nonlinearity concerning the extended state vector [52]. This situation can pose challenges, as the inclusion of numerous unknown parameters and the nonlinearity of the state equation may result in identification divergence [52]. For the issue of high dimensionality of state space vectors, this paper considers the updated physical parameters separately from the structural state space vector, reducing the parameter dimensions. For the estimation of the updated physical parameters, the MCMC method is introduced. As for the state equation, Taylor series expansion [53] is used for linearization in EKF and UKF. EKF utilizes the first-order Taylor expansion of nonlinear functions to approximate nonlinear functions, which has a poor effect on strongly nonlinear systems [54]. UKF addresses the limitations of the EKF by approximating the Gaussian probability density function using sigma points, but the filtering accuracy is generally limited to the third order at most [55, 56]. In this paper, the sparse grid interpolation method is employed to calculate recursive equations of state space vectors based on state equations. It can achieve Taylor precision of any order by changing the number of one-dimensional integral points. Subsequently, EnKF is employed to identify the state space vectors, while the MCMC method is utilized to calculate the likelihood function associated with the structural physical parameters. Building upon this, Bayesian inference is applied to derive the posterior distribution, providing a comprehensive probabilistic characterization of the identified parameters and their uncertainties.

The remainder of this paper is organized as follows. Section 2 presents the methodology. Sections 3 and 4 present two shaking table experiments to demonstrate the effectiveness of the proposed method. The final research findings are given in Section 5.

2. Methodology

2.1. State Space Models. For a multi degrees of freedom (MDOF) structure, the equation of motion is

$$M\ddot{x}(\theta) + F[x, \dot{x}, \theta] = Bf, \tag{1}$$

where M denotes the structural mass matrix. In general, the accurate estimation of the mass of a structure is available, so M is considered to be known. The vectors x, x, and $\ddot{x}$ denote the displacement, velocity, and acceleration, respectively, while θ represents the uncertain physical parameter. f denotes the external excitation, and B denotes the corresponding location matrix. $F[x, \dot{x}, \theta]$ is the nonlinear resilience vector. For the frame structure, $F[x, \dot{x}, \theta] = C\dot{x}(\theta) + Kx(\theta)$, where C, K represent the damping and stiffness matrices, respectively.

In the conventional EKF, the identification process involves simultaneous estimation of uncertain physical parameters and the state space vector by constructing an extended state space vector $X = \left\{x^T, \dot{x}^T, \theta^T\right\}^T$ [52]. Consequently, the state equation can be deduced from equation (1):

$$\dot{X} = \left\{M^{-1}\left[-C\dot{x}(\theta)\frac{\dot{x}}{0}Kx(\theta) + Bf\right]\right\} + w = g\left(\widehat{X}_k, \widehat{\theta}_k, f_k\right) + w. \tag{2}$$

where w denotes the zero-mean noise vector, and the subscript k denotes time $t = k \times \Delta t$ with Δt representing the time step. In the following text, the time will be denoted by the subscript k. Thus, the state space model can be expressed as [57]

$$\widetilde{X}_{k+1} = \widehat{X}_k + \int_{k\Delta t}^{(k+1)\Delta t} g\left(\widehat{X}_k, \widehat{\theta}_k, f_k\right)dt. \tag{3}$$

Considering the accelerometers deployed in the structure to measure acceleration, the observation can be formulated as follows:

$$\begin{aligned} y_{k+1} &= DM^{-1}\left(F\left[\dot{x}_k, x_k, \theta\right] + Bf_k\right) + v_k, \\ &= h\left(\widehat{X}_k, \widehat{\theta}_k, f_k\right) + v_k, \end{aligned} \tag{4}$$

where y_{k+1} is the measured acceleration response, and the observation operator $h(\cdot)$ denotes the observation y_k for the system state $\widehat{X}_k$ by mapping from the model space to the observation space. D represents the matrix associated with the accelerometer locations, while v_k is the zero-mean Gaussian white noise with a covariance matrix R_k [58]. The state space vector and the corresponding covariance matrix can be updated as

$$\begin{cases} K_{k+1} = \widetilde{P}_{k+1}H_{k+1}^T\left(H_{k+1}\widetilde{P}_{k+1}H_{k+1}^T + R_{k+1}\right)^{-1}, \\ \widehat{X}_{k+1} = \widetilde{X}_{k+1} + K_{k+1}\left(y_{k+1} - h\left(\widehat{X}_k, \widehat{\theta}_k, f_k\right)\right), \\ \widehat{P}_{k+1} = (I - K_{k+1}H_{k+1})\widetilde{P}_{k+1}. \end{cases} \tag{5}$$

where K_{k+1} is the Kalman gain.

2.2. Ensemble Kalman Filter. However, the calculation of EKF and UKF requires the analysis of the covariance matrix, but the calculation of the high-dimensional covariance matrix is computationally expensive and challenging to apply to complex real-world structures. To address this issue, the Ensemble Kalman Filter (EnKF) offers an alternative approach by utilizing sample moments to estimate the covariance matrix. This method effectively reduces the computational burden associated with computing the full covariance matrix in high-dimensional systems, allowing for a more robust treatment of non-Gaussian and nonlinear system behavior [59].

Here, a brief overview of the EnKF is presented. In EnKF, the state distribution is approximated using an ensemble, which represents a sample from the distribution. By utilizing this ensemble representation, dimension reduction is achieved, making it computationally feasible to handle even very high-dimensional systems [36]. Essentially, EnKF can be conceptualized as an approximation of the KF, offering a more practical solution for complex, high-dimensional scenarios [60].

$$p_{\text{enkf}}\left(x_k \mid y_{1:k-1}\right) = \mathcal{N}\left(x_k; \widehat{\mu}_k, \widehat{\Sigma}_k\right). \tag{6}$$

Assume that the ensemble $\widehat{X}_k^{(1)}, \ldots, \widehat{X}_k^{(N)}$ is a sample from the filtering distribution at time $t = k \times \Delta t$. Similar to the KF, the EnKF comprises a forecast step and an update step at every time point t [61]. For each ensemble, we perform the steps in Section 2.1 according to equations (3) and (4).

$$\widetilde{X}_{k+1}^{(i)} = \widehat{X}_k^{(i)} + \int_{k\Delta t}^{(k+1)\Delta t} g\left(\widehat{X}_k^{(i)}, \widehat{\theta}_k^{(i)}, f_k\right)dt, \tag{7}$$

$$y_{k+1}^{(i)} = DM^{-1}\left(F\left[\dot{x}_k, x_k, \theta\right] + Bf_k\right) + v_k = h\left(\widehat{X}_k^{(i)}, \widehat{\theta}_k^{(i)}, f_k\right) + v_k. \tag{8}$$

Then, compute estimates of the forecast mean and variance:

$$\begin{cases} \widetilde{\mu}_{k+1} = \dfrac{1}{n}\sum_{i}^{N} \widetilde{X}_{k+1}^{(i)}, \\ \widetilde{\sum}_{k+1} = \dfrac{1}{n-1}\sum_{i}^{N}\left(\widetilde{X}_{k+1}^{(i)} - \widetilde{\mu}_{k+1}\right)^2. \end{cases} \tag{9}$$

The Kalman gain matrix can be derided as $K_{k+1} = \widetilde{\sum}_{k+1} H_{k+1}^T (H_{k+1}\widetilde{\sum}_{k+1} H_{k+1}^T + R_{k+1})^{-1}$.

$$\widehat{X}_{k+1}^{(i)} = \widetilde{X}_{k+1}^{(i)} + K_{k+1}\left(y_{k+1} - h\left(\widehat{X}_k^{(i)}, \widehat{\theta}_k^{(i)}, f_k\right)\right). \tag{10}$$

In the EnKF method, the need to compute covariance directly at each step is circumvented. Instead, both the prior and the posterior distributions are represented with a set of samples.

2.3. Proposed SG-EnMCMC Method. By defining the 2d-dimensional state vector $X = \left\{x^T, \dot{x}^T\right\}^T$, equation (2) can be expressed as

$$\dot{X} = \begin{Bmatrix} \dot{x} \\ M^{-1}\left[-C\dot{x}(\theta) - Kx(\theta) + Bf\right] \end{Bmatrix} + w = g\left(\widehat{X}_k^{(i)}, \widehat{\theta}_k^{(i)}, f_k\right) + w. \tag{11}$$

Thus, the recurrence of X is given by $\widetilde{X}_{k+1}^{(i)} = \widehat{X}_k^{(i)} + \int_{k\Delta t}^{(k+1)\Delta t} g(\widehat{X}_k^{(i)}, \widehat{\theta}_k^{(i)}, f_k)\mathrm{d}t$. Since the expression for the state space model has a high-dimensional integral, this paper adopts the sparse grid interpolation method for simplification.

The sparse grid theory, initially proposed by mathematician Smolyak, serves as a numerical approach for integrating or interpolating high-dimensional functions [62]. Its core concept involves approximating the target model through a linear combination of multidimensional layered basis functions [63]. The Smolyak rule facilitates the establishment of a solution model for high-dimensional problems by utilizing the tensor product of various series basis functions in each dimension [64, 65]. In the 2d-dimensional case, the integral of interest is interpolated on an anisotropic grid Ω_l on $\Omega = [0, 1]^{2d}$ with different, but equidistant mesh size $h_l = (h_{l_1}, \ldots, h_{l_{2d}}) = 2^{-l} = (2^{-l_1}, \ldots, 2^{-l_{2d}})$, where $l = (l_1, \ldots, l_{2d}) \in \mathbb{N}^{2d}$ denote the grid refinement level. Therefore, the grid Ω_l consists of points

$$\theta_{l,j} = \left(\theta_{l_1,j_1}, \ldots, \theta_{l_{2d},j_{2d}}\right), \tag{12}$$

where $\theta_{l_t,j_t} = j_t \cdot h_{l_t} = j_t \cdot 2^{-l_t}$ and $j_t = 1, \ldots, 2^{l_t} - 1$, j_t odd, and $t \in \{1, \ldots, 2d\}$. To construct a hierarchical basis for interpolating $g(\widehat{X}_k, \widehat{\theta}_k, f_k)$, the hat function $\phi(\theta)$ is used to define for each grid point x_{l_t,j_t}, a basis function $\phi_{l_t,j_t}(\theta_{l_t,j_t})$. $\phi(\theta)$ and $\phi_{l_t,j_t}(\theta_{l_t,j_t})$ are given as follows:

$$\begin{aligned} \phi(\theta) &= \begin{cases} 1 - |\theta|, & \text{if } \theta \in [-1, 1], \\ 0, & \text{otherwise.} \end{cases} \\ \phi_{l_t,j_t}(\theta) &= \phi\left(\frac{\theta - j_t \cdot h_{l_t}}{h_{l_t}}\right), \end{aligned} \tag{13}$$

with $\phi_{l_t,j_t}(\theta_{l_t,j_t}) = 1$ and support $[\theta_{l_t,j_t} - h_{l_t}, \theta_{l_t,j_t} + h_{l_t}] = [(i_j - 1)h_{l_t}, (i_j + 1)h_{l_t}]$. The corresponding 2d-dimensional basis function $\phi_{l,i}(x)$ is expressed as the product of the basis functions: $\phi_{l,i}(\mathbf{x}) := \prod_{t=1}^{2d} \phi_{l_t,i_t}(x_t)$. To order the basis functions, the hierarchical difference spaces is

$$W_l := \mathrm{span}\left\{\phi_{l_t,j_t} : j_t \in I_t\right\}, \quad I_t = \left\{1 \le j_t \le 2^{l_t} - 1, j_t \text{ odd}, 1 \le t \le 2d\right\}. \tag{14}$$

The sum of the hierarchical difference spaces results in the function space [66].

$$V_l = \bigoplus_{k_1=1}^{l_1} \cdots \bigoplus_{k_{2d}=1}^{l_{2d}} W_k, \tag{15}$$

where $|l|_\infty = \max_{1 \le t \le d} \; l_t$. Consider a special case, which is an isotropic space $V_n := V_{(n,\ldots,n)} = \oplus_{|l|_\infty \le 2d} W_l$. In other words, $l_1 = l_2 = \cdots = l_{2d}$. The full Cartesian grid V_n has $(2^n + 1)^{2d}$ grid points. However, the approach for generating a sparse grid is to exclude the subspaces within the full grid space that contribute little [66]:

$$V_n = \bigoplus_{|l|_1 \le n+2d-1} W_l. \tag{16}$$

Unlike the full grid approach, which imposes restrictions on the maximum grid refinement levels across dimensions, the sum of these is restricted in the sparse grid. The sparse

grid employs a linear combination of low-level tensor products of univariate quadrature rules to approximate complex integrals [67, 68], and the number of points required is

$$|V_n| = \sum_{|l|_1 \le n+2d-1} 2^{|l-1|_1} = \sum_{j=2d}^{n+2d-1} 2^{j-2d} \cdot \sum_{|l|_1=i} 1 = \sum_{j=2d}^{n+2d-1} 2^{j-2d} \cdot \begin{pmatrix} j-1, \\ 2d-1. \end{pmatrix} = 2^n \cdot \frac{(n+2d-1)!}{(2d-1)!n!}, \tag{17}$$

which is much less than that of the full grid $(2^n+1)^{2d}$. When $l=3$, the difference between a full grid and a sparse grid is illustrated in Figure 2

Thus, the interpolate of $g(\hat{X}_k, \hat{\theta}_k, f_k)$ can be represented by

$$\int_{k\Delta t}^{(k+1)\Delta t} g\left(\hat{X}_k^{(i)}, \hat{\theta}_k^{(i)}, f_k\right) dt \approx u\left(\hat{\theta}_k^{(i)}\right) = \sum_{|l|_1 \le n+2d-1} \sum_{j \in I_l} c_{l,j} \cdot \phi_{l,j}\left(\hat{\theta}_k^{(i)}\right), \tag{18}$$

where $\phi_{l,j}$ is the basis function and $c_{l,j}$ denotes the hierarchical surpluses. Like the process of deriving $\phi_{l,j}(\hat{\theta}_k^{(i)})$, $c_{\underline{l},\underline{j}}$ in one dimension is first considered and given by

$$\begin{aligned} c_{\underline{l},\underline{j}} &= f\left(\theta_{\underline{l},\underline{j}}\right) - \frac{f\left(\theta_{\underline{l},\underline{j}} - h_l\right) + f\left(\theta_{\underline{l},\underline{j}} + h_l\right)}{2} = f\left(\theta_{\underline{l},\underline{j}}\right) - \frac{f\left(\theta_{\underline{l},\underline{j}-1}\right) + f\left(\theta_{\underline{l},\underline{j}+1}\right)}{2} \\ &= f\left(\theta_{\underline{l},\underline{j}}\right) - \frac{f\left(\theta_{\underline{l}-1,\left(\underline{j}-1\right)/2}\right) + f\left(\theta_{\underline{l}-1,\left(\underline{j}+1\right)/2}\right)}{2}, \end{aligned} \tag{19}$$

where $1 \le \underline{l} \le l_t$. Take a semicircle, for example, the interpolation process is illustrated in Figure 2(b). Figure 2(b) and equation (19) specify the change from level $l-1$ to level l. For simplification, equation (19) is rewritten as $c_{\underline{l},\underline{j}} = [-1/2\ 1\ -1/2]_{\underline{l},\underline{j}} f$. Then, the d-dimensional hierarchical surplus can be generalized as follows:

$$c_{l,j} = \left(\prod_{t=1}^{d} \left[-\frac{1}{2}\ 1\ -\frac{1}{2}\right]_{l_t,j_t}\right) f. \tag{20}$$

By adjusting the mesh size h, the sparse mesh interpolation here can achieve any accuracy, higher than EKF and UKF. Then, the state space model and the variance matrix can be derived as

$$\begin{cases} \tilde{X}_{k+1}^{(i)} = \hat{X}_k^{(i)} + \sum_{|l|_1 \le n+d-1} \sum_{j \in I_l} c_{l,j} \cdot \phi_{l,j}\left(\hat{\theta}_k^{(i)}\right), \\ \tilde{\mu}_{k+1} = \frac{1}{n} \sum_{i}^{N} \tilde{X}_{k+1}^{(i)} \\ \widetilde{\sum_{k+1}} = \frac{1}{N-1} \sum_{i}^{N} \left(\tilde{X}_{k+1}^{(i)} - \tilde{\mu}_{k+1}\right)^2. \end{cases} \tag{21}$$

The recursive estimation can be rewritten as

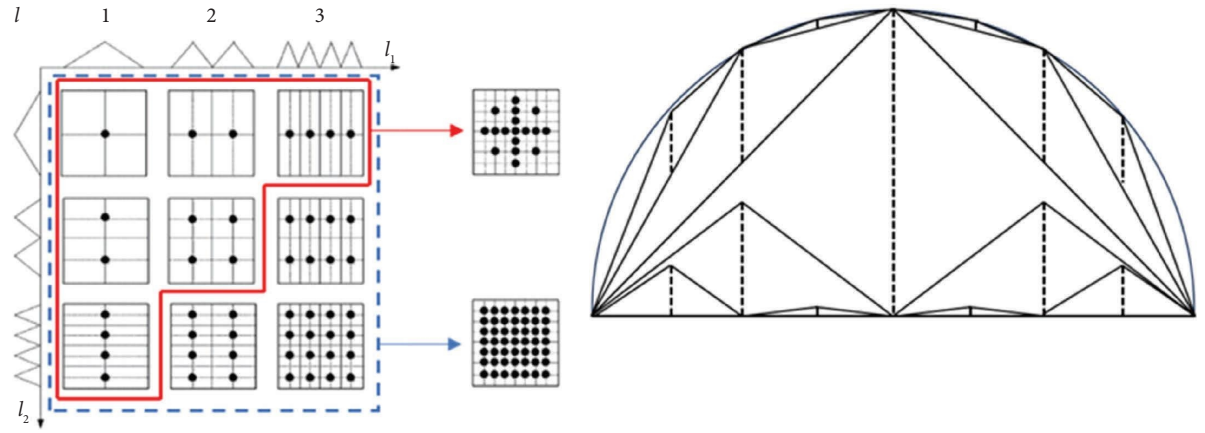

(a) (b)

FIGURE 2: Description of the sparse grid. (a) Comparison between a full grid and a sparse grid. (b) Example of interpolation for a semicircle.

$$\begin{cases} K_{k+1} = \widetilde{\sum_{k+1}} H_{k+1}^T \left(H_{k+1} \widetilde{\sum_{k+1}} H_{k+1}^T + R_{k+1} \right)^{-1}, \\ \widehat{X}_{k+1}^{(i)} = \widetilde{X}_{k+1}^{(i)} + K_{k+1} \left(y_{k+1} - h\left(\widehat{X}_k^{(i)}, \widehat{\theta}_k^{(i)}, f_k \right) \right). \end{cases} \tag{22}$$

Hence the filtering density is approximated by

$$p_{\text{enkf}}\left(x_k \mid y_{1:k}, \widehat{\theta}_k\right) = \mathcal{N}\left(x_k; \widehat{\mu}_k, \widehat{\Sigma}_k\right), \tag{23}$$

where $\widehat{\mu}_k = 1/n \sum_i^N \widehat{X}_k^{(i)}$, $\widehat{\Sigma}_k = 1/n - 1 \sum_i^N (\widehat{X}_k^{(i)} - \widehat{\mu}_k)^2$. As the number of ensemble members $N \longrightarrow \infty$, $p_{\text{enkf}}(x_k \mid y_{1:k}, \widehat{\theta}_k)$ converges to the true filtering distribution in a linear Gaussian state space model [69]. For a linear state model and finite N, the EnKF approximates the KF by substituting the mean and variance with their sample equivalents [70].

Based on EnKF, the likelihood estimate can be written in a sequential form:

$$L(\theta) = p(y_1 \mid x_1) p(x_1) \prod_{k=2}^{T} p(y_k \mid y_{1:k-1}, x_k) p(x_k \mid x_{k-1}, \theta_{k-1}). \tag{24}$$

From equation (8), an EnKF approximation of $p(y_k \mid y_{1:k-1}, x_k)$ is

$$p_{\text{enkf}}^N(y_k \mid y_{1:k-1}, x_k) = \mathcal{N}\left(H\widetilde{\mu}_k + DM^{-1}Bf_k; P\widetilde{\mu}_k, P \widetilde{\sum_k} P' + S \right), \tag{25}$$

which can be calculated for $t = 1, \ldots, T$, with the notation $p(y_1 \mid x_1) p(x_1) = p(y_1 \mid y_{1:0}, x_1) p(x_1 \mid x_0, \theta_0)$. Thus, the overall approximation is given by $\widehat{L}_{\text{enkf}}^N(\theta_k) = \prod_{k=1}^T p_{\text{enkf}}^N(y_k \mid y_{1:k-1}, x_k) p(x_k \mid x_{k-1}, \theta_{k-1})$. Then, the posterior distribution of uncertain physical parameters θ can be expressed as

$$\begin{aligned} p_{\text{enkf}}^N\left(\theta_T^{(s)} \mid y_{1:T}^{(s)}\right) &= \frac{1}{Z} \widehat{L}_{\text{enkf}}^N\left(\theta_T^{(s)}\right) p\left(\theta_1^{(s)}\right) \\ &= \frac{1}{Z} p(\theta_1) \prod_{t=2}^{T} p_{\text{enkf}}^N\left(y_k^{(s)} \mid y_{1:k-1}^{(s)}, x_k^{(s)}\right) p\left(x_k^{(s)} \mid x_{k-1}^{(s)}, \theta_{k-1}^{(s)}\right), \end{aligned} \tag{26}$$

where Z is the normalized constant (also called evidence) and $\{x_k^{(s)}\}_{s=1}^N$ and $\{\theta_k^{(s)}\}_{s=1}^N$ are the N samples at the previous time $k-1$. $\{x_k^{(s)}\}_{s=1}^N$ is sampled from $p_{\text{enkf}}(x_k^{(s)} \mid y_{1:k}^{(s)}, \widehat{\theta}_k^{(s)})$ following equation (23), and $\{\theta_k^{(s)}\}_{s=1}^N$ is obtained by the following resampling approach. The mean of samples at time $k-1$ is chosen as the initial sample of the chain at time k [71]. Subsequently, candidates $\theta_k^{(s)*}$ are generated by sampling from the proposal distribution centered on the previous point $\theta_k^{(s-1)}$. Then, these candidate parameters $\theta_k^{(s)*}$ are rejected or accepted according to the Metropolis algorithm. The acceptance rate is given by

$$\alpha_k^{(s)} = \frac{p_{\text{enkf}}^N\left(y_k^{(s)} \mid y_{1:k-1}^{(s)}, x_k^{(s)}\right) p\left(x_k^{(s)} \mid x_{k-1}^{(s)}, \theta_k^{(s)*}\right) q\left(\theta_{k-1}^{(s)} \mid \theta_k^{(s)*}\right)}{p_{\text{enkf}}^N\left(y_{k-1}^{(s)} \mid y_{1:k-2}^{(s)}, x_{k-1}^{(s)}\right) p\left(x_{k-1}^{(s)} \mid x_{k-2}^{(s)}, \theta_{k-1}^{(s)}\right) q\left(\theta_k^{(s)*} \mid \theta_{k-1}^{(s)}\right)}. \tag{27}$$

The process is followed by generating a uniform distribution in the interval (0,1) and selecting a number, u, randomly. If $u < \alpha_k$, the candidate is accepted, that is, $\theta_k^{(s)} = \theta_k^{(s)*}$, otherwise $\theta_k^{(s)} = \theta_{k-1}^{(s)}$. However, the above steps are specific to single-chain MCMC. Since there exist N samples $\{\theta_k^{(s)}\}_{s=1}^N$, the above process can be replaced by a resampling approach used in TMCMC [72]:

$$\theta_{k+1}^{(s)} = \theta_k^{(p)*} \text{ w. p. } \frac{\alpha_k^{(p)}}{\sum_{p=1}^N \alpha_k^{(p)}}, \quad p = 1, \ldots, N. \tag{28}$$

If N is large, $\{\theta_k^{(s)}\}_{s=1}^N$ will be distributed as the posterior distribution. The overall scheme is illustrated in the following Algorithm 1.

3. Case Study: Shaking Table Experiment

The proposed SG-EnMCMC method has been successfully implemented in a shaking table experiment conducted on a 3-storey reinforced concrete structure. The prototype of the test specimen featured a frame in the transverse direction (frame direction) and a frame-wall interacting system in the longitudinal direction (wall direction). The natural vibrational periods were determined to be 0.47 seconds and 0.69 seconds in the x- and y-directions, respectively. Additionally, the base shear coefficients were established at 0.12 and 0.09 in the x- and y-directions, respectively.

The test specimen, depicted in Figure 3, had plan dimensions of 4700 mm in the x-direction and 3000 mm in the y-direction, with a storey height of 2300 mm. The total height, encompassing the foundation beam, was measured at 7300 mm. The test model was scaled to 1/2 of the geometry of the prototype structure and adopted identical materials to the prototype, maintaining a scale ratio of 1.0 for stress and acceleration. The masses of the three-storey structures were 15.51 t, 15.32 t, and 14.66 t, respectively. Dynamic response data were acquired using strong zero-mean motion records, specifically the JMA Kobe records, which were scaled to peak ground accelerations of 0.07 g, representing the service-level earthquake for reinforced concrete, uniaxially applied in either the x- or y-directions. These seismic motions were applied first in the x-direction, denoted as Working Condition 1 (WC1), and then in the y-direction, denoted as Working Condition 2 (WC2). The bidirectional white Gaussian noise was introduced for system identification purposes before and after each seismic motion. The white noise had a bandpass frequency of 0.5–50 Hz and a duration of 240 s.

In the tests, the interstorey drift measurement is implemented by the computer vision-based measurement approach proposed by Cai et al. [73], as Figure 3 shows. A sampling frequency of 50 Hz was set in the cameras. The identified displacement time history is subjected to differentiation, yielding the corresponding acceleration time history. Subsequently, the proposed methodology is employed to estimate the physical parameters of the structure.

The acceleration obtained by loading the initial structure with white noise, along with the storey mass, can be used to calculate the storey shear. Additionally, by combining the displacement time history, the approximate undamaged storey stiffness k_{xi}^u and k_{yj}^u (i, $j = 1, 2, 3$) value is determined, which is listed in Table 1. The reference storey stiffness for each working condition is additionally determined through the application of a white noise load following seismic loading, employing this method. This paper defines the ratio of damaged storey stiffness to the undamaged storey stiffness θx_1, θx_1, θx_3, θy_1, θy_2, and θy_3 as the updated parameter ($\theta_{xi} = k_{xi}^d / k_{xi}^u$, $\theta_{yj} = k_{yj}^d / k_{yj}^u$), due to intuitively representing the damage degree of storey stiffness and the requirements for parameter normalization in sparse grid interpolation. For each working condition, the updated parameters are the unscaled storey stiffness in the same direction as the seismic motion. The parameters are assumed to be independent and identically distributed following uniform prior distributions U (0.7, 1). The damping of the structure adopts Rayleigh damping.

An ensemble of 500 members is drawn from the prior distributions and used to update the space state vector. Then, the state space vector is recursively calculated, and the mesh size $l = 6$. Based on the proposed method, displacement and storey stiffness of the building can be effectively identified. Figures 4 and 5 present qualitative comparisons of the estimated time history of storey drifts using different methods. The calculation of storey drifts time history involves the subtraction of the storey displacements from that of the preceding storey. In both working conditions, the drifts estimated by the proposed algorithm tend close to the reference drifts. In contrast, the drifts obtained by the EKF

Input: proposal Gaussian distribution $q(\theta \mid \theta^*)$; prior distribution $p(\theta)$; iteration steps T; number of ensemble N; for $i = 1, 2, \ldots, N$ sample $x_0^{(i)}$ from the initial state distribution; stiffness, mass, and damping matrices K, M, C
For $k = 1, \ldots, T$ do
(1) For the state recursion equation, use sparse grid interpolation for simplification, and compute $x_k^{(i)}$ from $x_{k-1}^{(i)}$
(2) Compute estimates of the forecast mean and variance $\widehat{\mu}_{k|k-1}$ and $\widehat{\Sigma}_{k|k-1}$
(3) Compute the EnKF approximation $p_{\text{enkf}}^N(y_k \mid y_{1:k-1}, \theta_k) = \mathcal{N}(H\widehat{\mu}_{k|k-1} + DM^{-1}Bf_k; P\widehat{\mu}_{k|k-1}, P\widehat{\Sigma}_{k|k-1}P' + S)$
(4) Compute the acceptance rate α_k and resample θ by equation (28)
(5) Compute the approximate Kalman gain, and update state vector by equation (22).
End

Algorithm 1: Proposed SG-EnMCMC method.

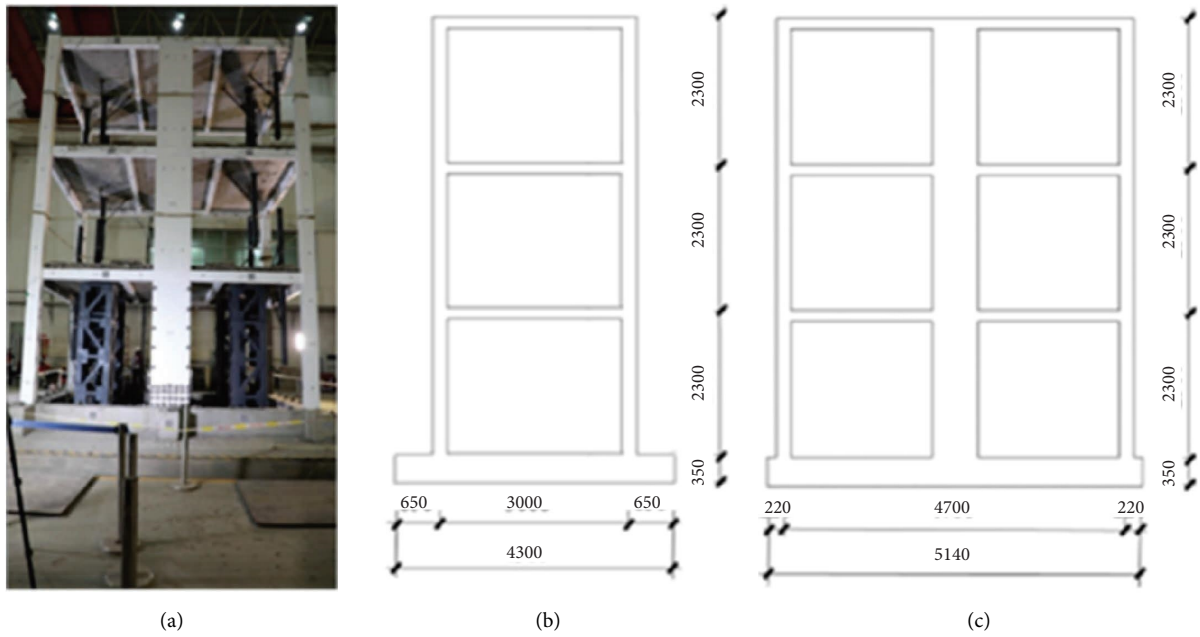

Figure 3: Shaking table experiment: (a) test specimen, (b) side view in x direction, and (c) side view in y direction.

Table 1: Initial mass and stiffness of each storey.

	Storey mass (ton)	Storey stiffness in x direction (kN/mm)	Storey stiffness in y direction (kN/mm)
1st storey	4.75	20.85	5.48
2nd storey	6.64	9.23	3.29
3rd storey	7.95	8.37	4.21

method show a relatively larger deviation from the reference drifts, particularly in the y direction, which seems obvious after 10 s. Overall, from a qualitative standpoint, the proposed algorithm exhibits superior performance compared to the conventional EKF method.

Figure 6 demonstrates the convergences of the identified storey stiffness θ_{x1} and θ_{y2} by the proposed method and the EKF due to space limitations. This figure reflects the trend of the most probable value (MPV) in the identification parameter samples obtained at each step of the MCMC iteration using two methods, with black lines representing reference data. It is noteworthy that the stiffness parameters identified through both methods exhibit rapid convergence, indicating that the duration of the measurement responses needed for accurate parameter estimation is relatively short. However, the proposed method converges earlier than the EKF method. Besides, the EKF method is more violent and susceptible than the proposed method in the initial steps. This efficiency in convergence suggests the effectiveness and efficiency of the employed identification methods in capturing the essential structural characteristics. A conclusion can be drawn that the proposed method is superior to EKF-based model updating in terms of convergence speed.

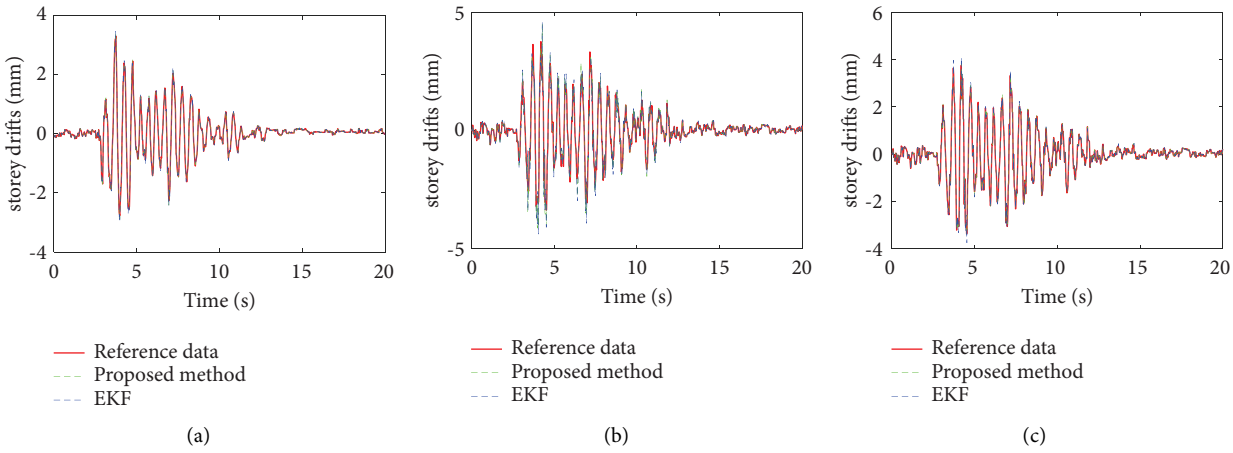

Figure 4: Interstorey drift responses in WC1 in (a) the 1st storey, (b) the 2nd storey, and (c) the 3rd storey.

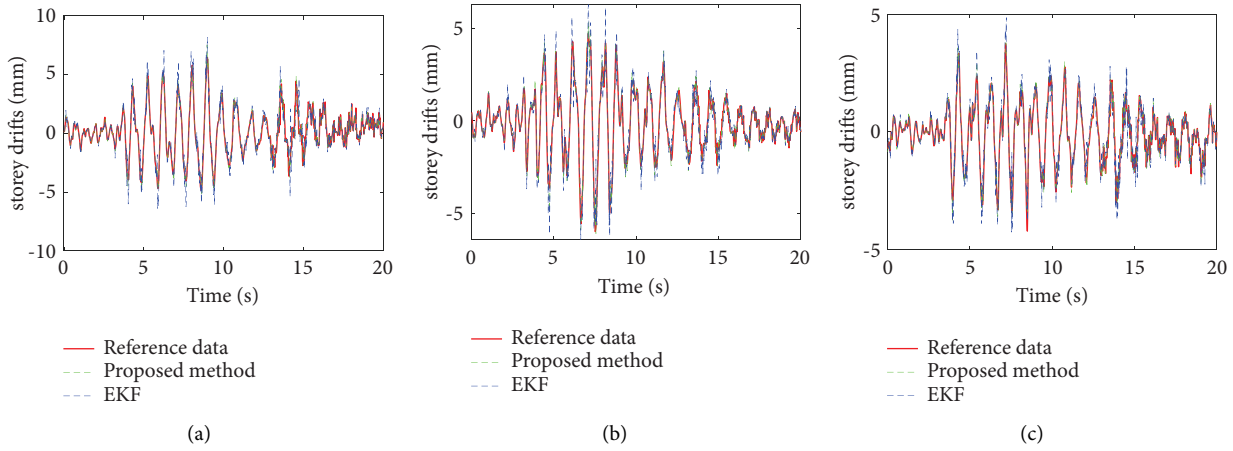

Figure 5: Interstorey drift responses in WC2 in (a) the 1st storey, (b) the 2nd storey, and (c) the 3rd storey.

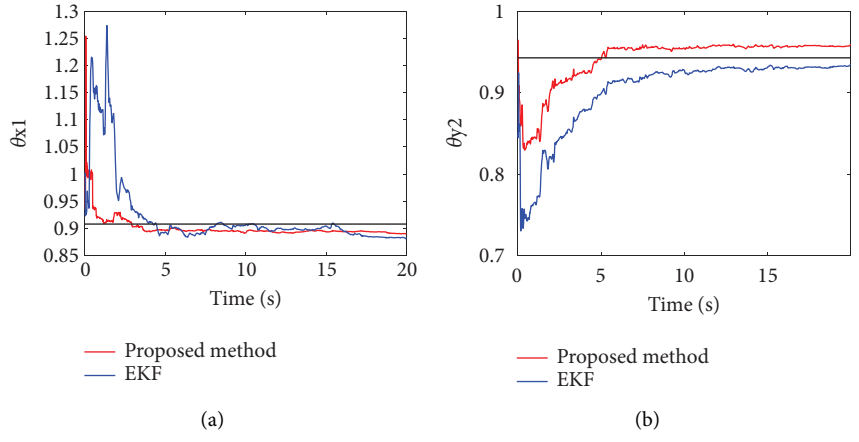

Figure 6: Convergences of the identified storey stiffness (a) theta_x1 and (b) theta_y2.

The most probable value (MPV) and the variance in the two working conditions are presented in Table 2. In WC1, the identified MPV of unscaled storey stiffness using the proposed method is 0.8946, 0.9315, and 0.9558, while that of EKF is 0.8756, 0.9382, and 0.9324. The reference data are 0.9079, 0.9179, and 0.9424. In WC2, the identified MPV of unscaled storey stiffness using the proposed method is 0.9396, 0.9577, and 0.9189, while that of EKF is 0.9474,

Table 2: MPV and variance of the updated parameters in the shaking table experiment.

Working condition	Variables	Reference data	Kalman filter		Proposed method	
			MPV	Variance	MPV	Variance
WC1	θx_1	0.9079	0.8756	0.1369	0.8946	0.1034
	θx_2	0.9197	0.9382	0.1427	0.9315	0.1189
	θx_3	0.9424	0.9324	0.1307	0.9558	0.1068
WC2	θy_1	0.9147	0.9474	0.1467	0.9396	0.0967
	θy_2	0.9428	0.9287	0.1512	0.9577	0.1012
	θy_3	0.8926	0.9245	0.1447	0.9189	0.0987

0.9287, and 0.9245. The reference data are 0.9147, 0.9428, and 0.8926. Additionally, the parameter variance identified by the proposed method is also smaller than that of the EKF method.

Figures 7 and 8 show the marginal posterior PDFs of the parameters of the two methods under the two working conditions. It is evident that when the proposed method is employed, the spread of the updated parameters is reduced, confirming less variance, which is consistent with the conclusion obtained from Table 2. From observations in Table 2 and Figures 7 and 8, it can be concluded that updated parameters for the two working conditions have been well identified and the structural damage can be quantified. The proposed method effectively enables parameter identification and damage quantification, which outperforms the EKF method in convergence speed and identified accuracy.

4. Case Study: Full-Scale Nonstructural Element Simulator on Shake Table (NEST)

To further evaluate the viability of the proposed SG-EnMCMC algorithm, a three-floor test specimen called the NEST is also conducted. As illustrated in Figure 9, the NEST substructure loading unit is a steel structure system comprising a three-tier platform configuration. Four large friction pendulum supports, each with a diameter of 1300 mm, are strategically positioned between the first-floor platform and the vibrating table. Separating the first-floor and second-floor platforms is a steel support frame, divided into upper and lower sections by four natural rubber supports. The second-floor structure incorporates four 450 mm diameter friction pendulum supports, along with a series of horizontal springs arranged around the frame's perimeter, to provide additional lateral stiffness.

The loading device itself has a weight of 10.36 tons, significantly below the maximum load capacity of the shaking table, which is rated for 30 tons. This surplus capacity allows for the adjustment of the mass of each platform within the loading device through counterweights, as well as the installation of nonstructural components for testing. Each platform within the test frame features reserved holes (as depicted in Figure 9), enabling the addition of counterweights to fine-tune the mass of the NEST layers within a certain range. Moreover, the stiffness of each NEST layer can be adjusted within a defined range by replacing the isolation supports located between the platforms.

Flexibility in design is a notable feature of the NEST system. It allows for the locking together of layers, both among themselves and between the first layer and the shaking table. This adaptable configuration permits the NEST system to be adjusted to accommodate single-layer, two-layer, or three-layer test frames, depending on the specific requirements of various application scenarios.

A full-scale trial was performed on the 5 m-by-5 m shake table. To ensure the rigidity of the system during vibration, the braced steel frame exhibited a significantly high stiffness. Table 3 provides details on the floor masses, and storey stiffnesses are identical in both directions. The input is derived from the recorded intense ground motion data at the MZQ station during the 2008 M8.0 Wenchuan earthquake. This seismic record is notable for its pulse-like characteristics and the presence of abundant long-period content.

Four three-way acceleration sensors are arranged in the first, second, and third storey of the shaking table and test frame. The interstorey displacement of the first and second floor of the test frame is measured by a specially arranged interstorey displacement meter. Throughout the shaking period, the displacements and the accelerations of each storey were meticulously recorded using accelerometers and displacement transducers. The data acquisition occurred at a high-frequency interval of 0.001 seconds to capture precise and detailed information about the structural response. Subsequently, during the data processing phase, the collected data underwent resampling to a frequency of 50 Hz. The acceleration obtained by loading the initial structure with white noise, along with the storey mass, can be used to calculate the storey shear. Additionally, by combining the displacement time history, the approximate undamaged interstorey stiffness k_i^u $(i = 1, 2, 3)$ value is determined. In order to obtain the damage degree of storey stiffness intuitively, this paper defines the ratio of damaged interstorey stiffness to the undamaged storey stiffness θ_1, θ_2, and θ_3 as the updated parameter $(\theta_i = k_i^d/k_i^u)$. The parameters are assumed to be independent and identically distributed following uniform distributions U (0.7, 1). The damping of the structure adopts Rayleigh damping.

An ensemble comprising 500 members is drawn from the prior distributions and utilized to update the state space vector. The state space vector is then iteratively calculated with a mesh size of $l = 6$. Figure 10 presents qualitative comparisons of the estimated time history of storey drifts using two methods. The drifts estimated by the proposed method closely align with the reference data. In contrast, drifts obtained using the EKF method deviate a little largely from the reference data. A similar conclusion is drawn that the proposed method exhibits superior performance in convergence compared to the conventional EKF method.

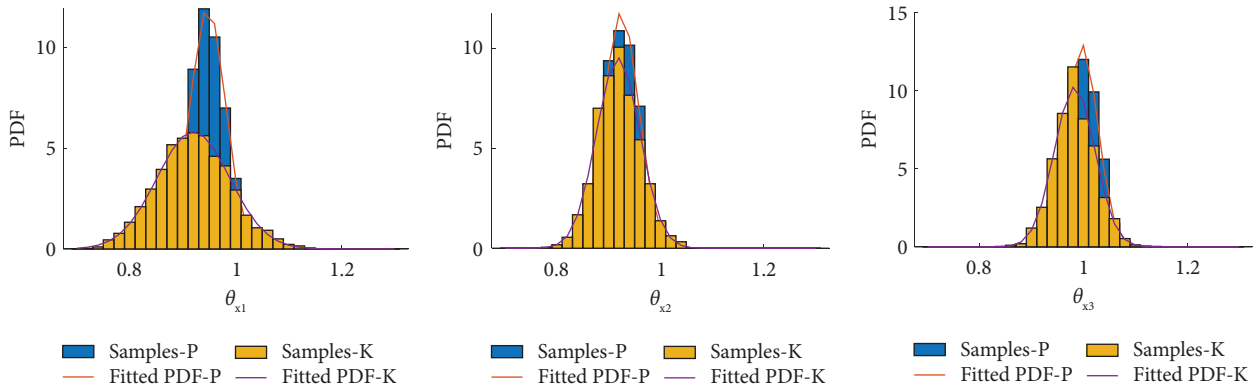

Figure 7: Updated parameters in x direction.

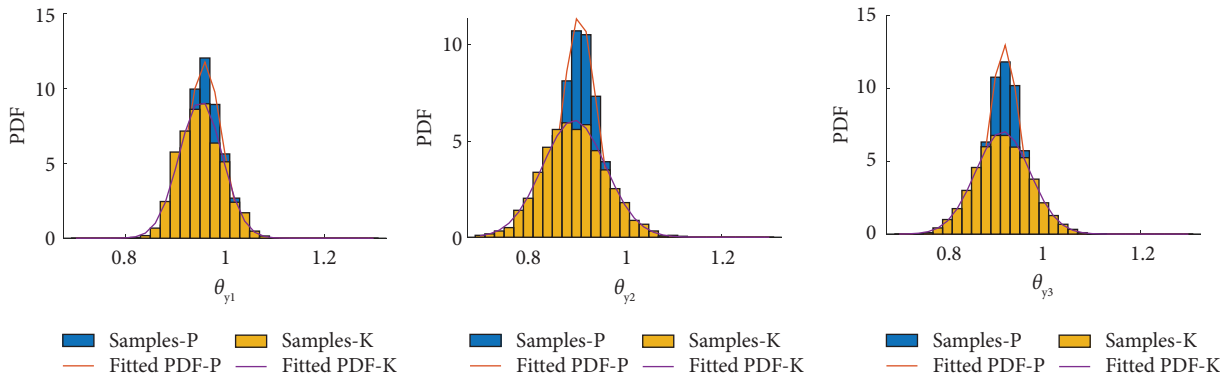

Figure 8: Updated parameters in y direction.

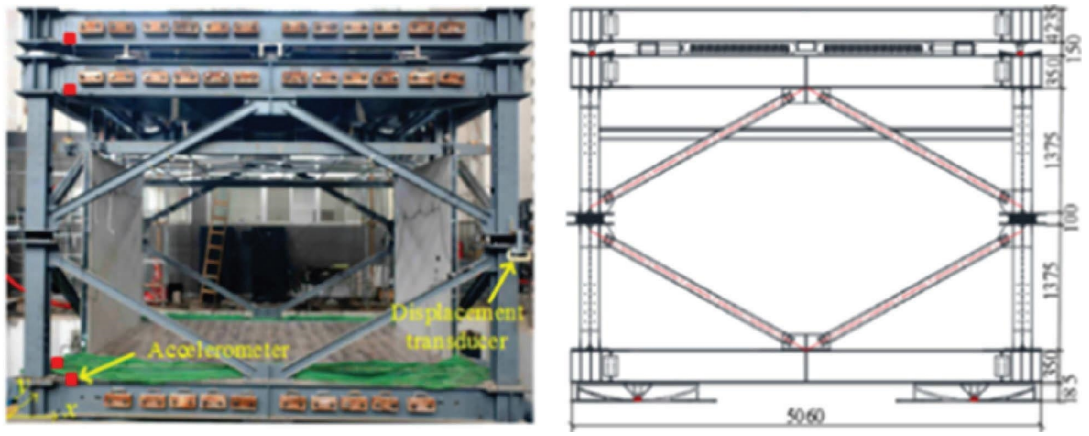

(a) (b)

Figure 9: Continued.

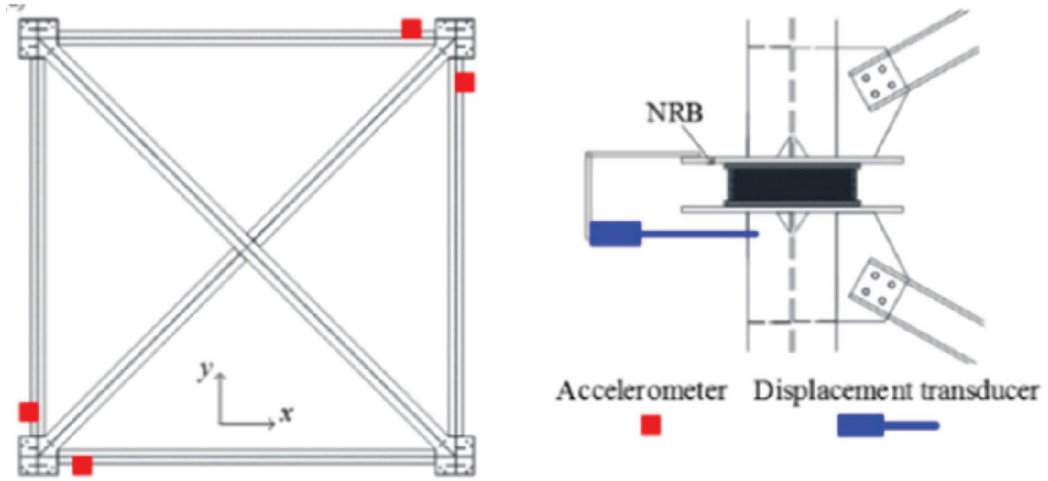

(c) (d)

Figure 9: Overview and illustrations of the test specimen: (a) general view, (b) side view in the x direction, (c) arrangement of the displacement transducer, and (d) arrangement of the accelerometers.

Table 3: Mass and stiffness of each storey of substructure loading device.

	Storey mass (ton)	Storey stiffness (kN/mm)
1st storey	4.75	0.118
2nd storey	6.64	1.995
3rd storey	7.95	0.239

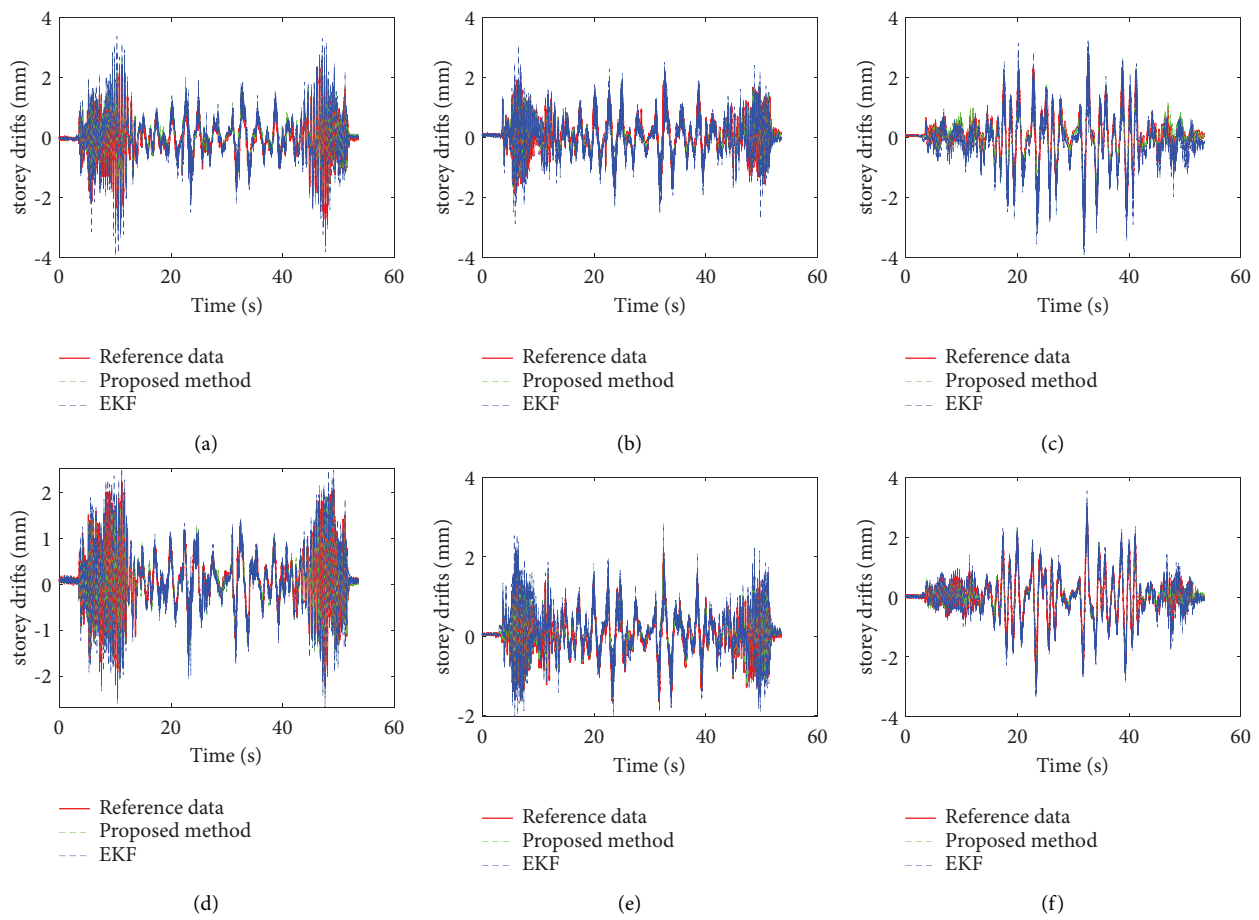

Figure 10: Interstorey drift responses in (a) x direction of the 1st storey, (b) x direction of the 2nd storey, (c) x direction of the 3rd storey, (d) y direction of the 1st storey, (e) y direction of the 2nd storey, and (f) y direction of the 3rd storey.

Table 4: MPV and variance of the updated parameters in the Nest.

Variables	Reference data	Kalman filter		Propose method	
		MPV	Variance	MPV	Variance
k_1	0.9318	0.9056	0.1279	0.9252	0.1134
k_2	0.9467	0.9324	0.1465	0.9421	0.0967
k_3	0.9157	0.8918	0.1298	0.9007	0.0994

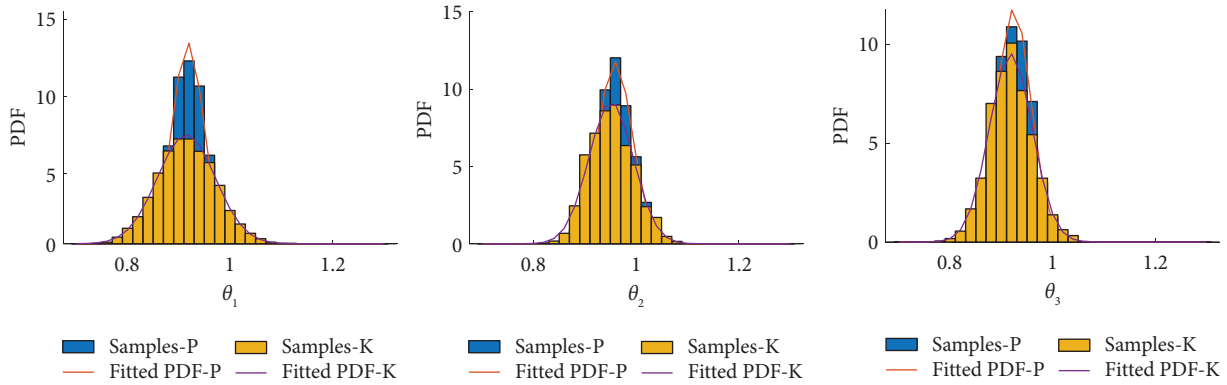

Figure 11: Updated parameters.

Table 4 presents the MPV and variance. The identified MPV of unscaled storey stiffness using the proposed method is 0.9252, 0.9421, and 0.9007, while that of EKF is 0.9056, 0.9324, and 0.8918. The reference data are 0.9318, 0.9467, and 0.9157. The posterior variance of the proposed method is 0.1134, 0.0967, and 0.0994, while that of EKF is 0.1279, 0.1465, and 0.1298. Additionally, the parameter variance identified by the proposed method is smaller than that of the EKF method.

Figure 11 displays the marginal posterior PDFs of the parameters for both methods. It is evident that the use of the proposed method results in a reduced spread of the updated parameters, confirming lower variance, which is consistent with the conclusion drawn from Table 4. Observations from Table 4 and Figure 11 lead to the conclusion that parameters for the two working conditions have been effectively identified, enabling quantification of structural damage. The proposed method proves to be efficient in parameter identification and damage quantification, surpassing the EKF method in terms of convergence speed and identified accuracy.

5. Conclusion

A novel SG-EnMCMC method based on the sparse grid interpolation, the ensemble Kalman filter, and MCMC is proposed for model updating and damage identification. The sparse grid method and EnKF are used to simplify the calculation of state space vectors and state equations, ensuring their applicability in high-dimensional and nonlinear situations. By introducing the EnKF method, the estimation of the updated physical parameters is transformed into an MCMC process. The efficiency and accuracy of the proposed SG-EnMCMC method are assessed through validation in two shaking table experiments. Results indicate its ability to effectively identify physical parameters, demonstrating superiority over the traditional Extended Kalman Filter (EKF).

Data Availability

The data used to support the findings of this study are included within the article.

Conflicts of Interest

The authors declare that they have no conflicts of interest.

Acknowledgments

This work was supported by the National Key R&D Program of China (2023YFC3081300) and the National Natural Science Foundation of China (52311540150 and 52238011). All sources of support are gratefully acknowledged.

References

[1] M. Flah, I. Nunez, W. Ben Chaabene, and M. L. Nehdi, "Machine learning algorithms in civil structural health monitoring: a systematic review," *Archives of Computational Methods in Engineering*, vol. 28, no. 4, pp. 2621–2643, 2021.

[2] W. Y. He, S. Zhu, and W. X. Ren, "Progressive damage detection of thin plate structures using wavelet finite element model updating," *Smart Structures and Systems*, vol. 22, no. 3, pp. 277–290, 2018.

[3] A. Güemes, A. Fernandez-Lopez, A. R. Pozo, and J. Sierra-Pérez, "Structural health monitoring for advanced composite structures: a review," *Journal of Composites Science*, vol. 4, no. 1, p. 13, 2020.

[4] Y. Zhang, K. Wei, Z. H. Shen, X. W. Bai, X. Z. Lu, and C. G. Soares, "Economic impact of typhoon-induced wind

disasters on port operations: a case study of ports in China," *International Journal of Disaster Risk Reduction*, vol. 50, Article ID 101719, 2020.

[5] H. Sarmadi, A. Entezami, B. Saeedi Razavi, and K. V. Yuen, "Ensemble learning-based structural health monitoring by Mahalanobis distance metrics," *Structural Control and Health Monitoring*, vol. 28, no. 2, Article ID e2663, 2021.

[6] Y. Zhang, C. W. Kim, K. F. Tee, A. Garg, and A. Garg, "Long-term health monitoring for deteriorated bridge structures based on Copula theory," *Smart Structures and Systems*, vol. 21, no. 2, pp. 171–185, 2018.

[7] M. Abdar, F. Pourpanah, S. Hussain et al., "A review of uncertainty quantification in deep learning: techniques, applications and challenges," *Information Fusion*, vol. 76, pp. 243–297, 2021.

[8] E. Hüllermeier and W. Waegeman, "Aleatoric and epistemic uncertainty in machine learning: an introduction to concepts and methods," *Machine Learning*, vol. 110, no. 3, pp. 457–506, 2021.

[9] M. D. Packard and B. B. Clark, "Mitigating versus managing epistemic and aleatory uncertainty," *Academy of Management Review*, vol. 45, no. 4, pp. 872–876, 2020.

[10] F. J. Pallarés, M. Betti, G. Bartoli, and L. Pallarés, "Structural health monitoring (SHM) and Nondestructive testing (NDT) of slender masonry structures: a practical review," *Construction and Building Materials*, vol. 297, Article ID 123768, 2021.

[11] S. W. F. de Rezende, J. D. R. V. de Moura, R. M. F. Neto, C. A. Gallo, and V. Steffen, "Convolutional neural network and impedance-based SHM applied to damage detection," *Engineering Research Express*, vol. 2, no. 3, Article ID 035031, 2020.

[12] E. J. Cai and Y. Zhang, "Gaussian mixture model based phase prior learning for video motion estimation," *Mechanical Systems and Signal Processing*, vol. 175, Article ID 109103, 2022.

[13] K. Erazo and E. M. Hernandez, "Bayesian model–data fusion for mechanistic postearthquake damage assessment of building structures," *Journal of Engineering Mechanics*, vol. 142, no. 9, Article ID 04016062, 2016.

[14] S. Nagarajaiah and K. Erazo, "Structural monitoring and identification of civil infrastructure in the United States," *Structural Monitoring and Maintenance*, vol. 3, no. 1, pp. 51–69, 2016.

[15] R. Abbasnia, A. Mirzaee, and M. Shayanfar, "Simultaneous identification of damage in bridge under moving mass by Adjoint variable method," *Smart Structures and Systems*, vol. 21, no. 4, pp. 449–467, 2018.

[16] T. N. Hoa, S. Khatir, G. D. Roeck, N. N. Long, B. T. Thanh, and M. A. Wahab, "An efficient approach for model updating of a large-scale cable-stayed bridge using ambient vibration measurements combined with a hybrid metaheuristic search algorithm," *Smart Structures and Systems*, vol. 25, no. 4, 2020.

[17] C.-Z. Dong and F. N. Catbas, "A review of computer vision–based structural health monitoring at local and global levels," *Structural Health Monitoring*, vol. 20, no. 2, pp. 692–743, 2021.

[18] Q. Han, P. Ni, X. Du, H. Zhou, and X. Cheng, "Computationally efficient Bayesian inference for probabilistic model updating with polynomial chaos and Gibbs sampling," *Structural Control and Health Monitoring*, vol. 29, no. 6, Article ID e2936, 2022.

[19] Y. M. Zhang, H. Wang, and J. X. Mao, "A Bayesian neural network approach for probabilistic model updating using incomplete modal data," *Structural Control and Health Monitoring*, vol. 29, no. 10, Article ID e3030, 2022.

[20] S. Ereiz, I. Duvnjak, and J. F. Jiménez-Alonso, "Review of finite element model updating methods for structural applications," *Paper presented at the Structures*, vol. 41, 2022.

[21] J. Jang and A. W. Smyth, "Model updating of a full-scale FE model with nonlinear constraint equations and sensitivity-based cluster analysis for updating parameters," *Mechanical Systems and Signal Processing*, vol. 83, pp. 337–355, 2017.

[22] Z. Zhang and C. Sun, "Structural damage identification via physics-guided machine learning: a methodology integrating pattern recognition with finite element model updating," *Structural Health Monitoring*, vol. 20, no. 4, pp. 1675–1688, 2021.

[23] S. A. Alabi, Q. Hu, H. F. Lam, and H. P. Zhu, "Bayesian ballast damage detection utilizing a modified evolutionary algorithm," *Smart Structures and Systems*, vol. 21, no. 4, pp. 435–448, 2018.

[24] G. W. Lin, Y. Zhang, and Q. Z. Liao, "Developing efficient model updating approaches for different structural complexity- an ensemble learning and uncertainty quantifications," *Smart Structures and Systems*, vol. 29, no. 2, pp. 321–336, 2021.

[25] H. Tran-Ngoc, S. Khatir, G. De Roeck, T. Bui-Tien, L. Nguyen-Ngoc, and M. Abdel Wahab, "Model updating for Nam O bridge using particle swarm optimization algorithm and genetic algorithm," *Sensors*, vol. 18, no. 12, p. 4131, 2018.

[26] S. Baisthakur and A. Chakraborty, "Modified Hamiltonian Monte Carlo-based Bayesian finite element model updating of steel truss bridge," *Structural Control and Health Monitoring*, vol. 27, no. 8, Article ID e2556, 2020.

[27] J. L. Beck and L. S. Katafygiotis, "Updating models and their uncertainties. I: Bayesian statistical framework," *Journal of Engineering Mechanics*, vol. 124, no. 4, pp. 455–461, 1998.

[28] S. H. Cheung and J. L. Beck, "Bayesian model updating using hybrid Monte Carlo simulation with application to structural dynamic models with many uncertain parameters," *Journal of Engineering Mechanics*, vol. 135, no. 4, pp. 243–255, 2009.

[29] N. F. Alkayem, M. S. Cao, Y. F. Zhang, M. Bayat, and Z. Q. Su, "Structural damage detection using finite element model updating with evolutionary algorithms: a survey," *Neural Computing and Applications*, vol. 30, no. 2, pp. 389–411, 2018.

[30] J. Hu and J. H. Yang, "Operational modal analysis and Bayesian model updating of a coupled building," *International Journal of Structural Stability and Dynamics*, vol. 19, no. 01, Article ID 1940012, 2018.

[31] Y. Zhang, C. W. Kim, and J. M. Lin, "Removing environmental influences in health monitoring for steel bridges through copula approaches," *International Journal of Steel Structures*, vol. 19, no. 3, pp. 888–895, 2019.

[32] J. D. Collins, G. C. Hart, T. K. Hasselman, and B. Kennedy, "Statistical identification of structures," *American Institute of Aeronautics and Astronautics Journal*, vol. 12, no. 2, pp. 185–190, 1974.

[33] D. Li and J. Zhang, "Stochastic finite element model updating through Bayesian approach with unscented transform," *Structural Control and Health Monitoring*, vol. 29, no. 8, Article ID e2972, 2022.

[34] M. K. Lo and Y. F. Leung, "Bayesian updating of subsurface spatial variability for improved prediction of braced

excavation response," *Canadian Geotechnical Journal*, vol. 56, no. 8, pp. 1169–1183, 2019.

[35] Y. Yuan, F. T. Au, D. Yang, and J. Zhang, "Active learning structural model updating of a multisensory system based on Kriging method and Bayesian inference," *Computer-Aided Civil and Infrastructure Engineering*, vol. 38, no. 3, pp. 353–371, 2023.

[36] J. Li, X. Zhu, and J. Guo, "Enhanced drive-by bridge modal identification via dual Kalman filter and singular spectrum analysis," *Structural Control and Health Monitoring*, vol. 29, no. 5, Article ID e2927, 2022.

[37] Y. Liu, L. Wang, and M. Li, "Kalman filter–random forest-based method of dynamic load identification for structures with interval uncertainties," *Structural Control and Health Monitoring*, vol. 29, no. 5, Article ID e2935, 2022.

[38] P. Ni, Y. Xia, J. Li, and H. Hao, "Improved decentralized structural identification with output-only measurements," *Measurement*, vol. 122, pp. 597–610, 2018.

[39] C. Urrea and R. Agramonte, "Kalman filter: historical overview and review of its use in robotics 60 years after its creation," *Journal of Sensors*, vol. 2021, Article ID 9674015, 21 pages, 2021.

[40] G. Reina and A. Messina, "Vehicle dynamics estimation via augmented extended kalman filtering," *Measurement*, vol. 133, pp. 383–395, 2019.

[41] T. Kim and T.-H. Park, "Extended Kalman filter (EKF) design for vehicle position tracking using reliability function of radar and lidar," *Sensors*, vol. 20, no. 15, p. 4126, 2020.

[42] L. Guo, Y. Ding, Z. Wang, G. Xu, and B. Wu, "A dynamic load estimation method for nonlinear structures with unscented Kalman filter," *Mechanical Systems and Signal Processing*, vol. 101, pp. 254–273, 2018.

[43] M. Das, A. Dey, S. Sadhu, and T. K. Ghoshal, "Adaptive central difference filter for non-linear state estimation," *Institution of Engineering and Technology Science, Measurement and Technology*, vol. 9, no. 6, pp. 728–733, 2015.

[44] R. V. Garcia, P. C. P. M. Pardal, H. Kuga, and M. Zanardi, "Nonlinear filtering for sequential spacecraft attitude estimation with real data: cubature kalman filter, unscented kalman filter and extended kalman filter," *Advances in Space Research*, vol. 63, no. 2, pp. 1038–1050, 2019.

[45] T. J. Cocucci, M. Pulido, M. Lucini, and P. Tandeo, "Model error covariance estimation in particle and ensemble Kalman filters using an online expectation–maximization algorithm," *Quarterly Journal of the Royal Meteorological Society*, vol. 147, no. 734, pp. 526–543, 2021.

[46] I. Ullah, Y. Shen, X. Su, C. Esposito, and C. Choi, "A localization based on unscented Kalman filter and particle filter localization algorithms," *IEEE Access*, vol. 8, pp. 2233–2246, 2020.

[47] X. Lai, Y. Huang, X. Han, H. Gu, and Y. Zheng, "A novel method for state of energy estimation of lithium-ion batteries using particle filter and extended Kalman filter," *Journal of Energy Storage*, vol. 43, Article ID 103269, 2021.

[48] G. Evensen, "Sequential data assimilation with a nonlinear quasi-geostrophic model using Monte Carlo methods to forecast error statistics," *Journal of Geophysical Research: Oceans*, vol. 99, no. C5, pp. 10143–10162, 1994.

[49] Y. Li, B. Xiong, D. M. Vilathgamuwa, Z. Wei, C. Xie, and C. Zou, "Constrained ensemble Kalman filter for distributed electrochemical state estimation of lithium-ion batteries," *IEEE Transactions on Industrial Informatics*, vol. 17, no. 1, pp. 240–250, 2021.

[50] D. Sen, K. Erazo, and S. Nagarajaiah, "Bayesian estimation of acoustic emissions source in plate structures using particle-based stochastic filtering," *Structural Control and Health Monitoring*, vol. 24, no. 11, Article ID e2005, 2017.

[51] P. J. Van Leeuwen, "A consistent interpretation of the stochastic version of the Ensemble Kalman Filter," *Quarterly Journal of the Royal Meteorological Society*, vol. 146, no. 731, pp. 2815–2825, 2020.

[52] Y. Lei, F. Chen, and H. Zhou, "An algorithm based on two-step Kalman filter for intelligent structural damage detection," *Structural Control and Health Monitoring*, vol. 22, no. 4, pp. 694–706, 2015.

[53] Y. Cui, Y. Zhang, Y. Huang, Z. Wang, and H. Fu, "Novel WiFi/MEMS integrated indoor navigation system based on two-stage EKF," *Micromachines*, vol. 10, no. 3, p. 198, 2019.

[54] Y. Lei, J. Lai, J. Huang, and C. Qi, "A generalized extended Kalman particle filter with unknown input for nonlinear system-input identification under non-Gaussian measurement noises," *Structural Control and Health Monitoring*, vol. 29, no. 12, Article ID e3139, 2022.

[55] P. S. Madhukar and L. Prasad, "State estimation using extended kalman filter and unscented kalman filter," in *Proceedings of the Paper Presented at the 2020 International Conference on Emerging Trends in Communication, Control and Computing (ICONC3)*, Lakshmangarh, India, February 2020.

[56] S. Patnaik, J. Wang, Z. Yu, and N. Dey, "Recent developments in mechatronics and intelligent robotics proceedings of ICMIR 2019," *Proceedings of International Conference on Mechatronics and Intelligent Robotics*, vol. 1, 2019.

[57] J. Brumm, D. Mikushin, S. Scheidegger, and O. Schenk, "Scalable high-dimensional dynamic stochastic economic modeling," *Journal of Computational Science*, vol. 11, pp. 12–25, 2015.

[58] Y. Lei, H. Zhou, and Z. L. Lai, "A computationally efficient algorithm for real-time tracking the abrupt stiffness degradations of structural elements," *Computer-Aided Civil and Infrastructure Engineering*, vol. 31, no. 6, pp. 465–480, 2016.

[59] P. K. Paul, A. Dutta, and S. K. Deb, "Comparison of the performance of nonlinear Kalman filter based algorithms for state-parameter identification of base isolated structures," *Structural Control and Health Monitoring*, vol. 29, no. 10, Article ID e3029, 2022.

[60] E. Calvello, S. Reich, and A. M. Stuart, "Ensemble Kalman methods: a mean field perspective," *arXiv preprint arXiv:2209*, vol. 11371, 2022.

[61] M. Katzfuss, J. R. Stroud, and C. K. Wikle, "Understanding the ensemble Kalman filter," *The American Statistician*, vol. 70, no. 4, pp. 350–357, 2016.

[62] S. A. Smolyak, "Quadrature and interpolation formulas for tensor products of certain classes of functions," *Paper Presented at the Doklady Akademii Nauk*, vol. 148, 1963.

[63] D. Butnaru, B. Peherstorfer, H.-J. Bungartz, and D. Pflüger, "Fast insight into high-dimensional parametrized simulation data," in *Proceedings of the Paper Presented at the 2012 11th International Conference on Machine Learning and Applications*, Boca Raton, FL, USA, December 2012.

[64] B. Gao, G. Hu, Y. Zhong, and X. Zhu, "Distributed state fusion using sparse-grid quadrature filter with application to INS/CNS/GNSS integration," *IEEE Sensors Journal*, vol. 22, no. 4, pp. 3430–3441, 2022.

[65] J. Wu, D. Zhang, C. Jiang, X. Han, and Q. Li, "On reliability analysis method through rotational sparse grid nodes,"

Mechanical Systems and Signal Processing, vol. 147, Article ID 107106, 2021.

[66] J. Brumm and S. Scheidegger, "Using adaptive sparse grids to solve high-dimensional dynamic models," *Econometrica*, vol. 85, no. 5, pp. 1575–1612, 2017.

[67] B. Jia, M. Xin, and Y. Cheng, "Sparse-grid quadrature nonlinear filtering," *Automatica*, vol. 48, no. 2, pp. 327–341, 2012.

[68] C. Qian, C. Song, S. Li, Q. Chen, and J. Guo, "Algorithm of Gaussian sum filter based on SGQF for nonlinear non-Gaussian models," *International Journal of Control, Automation and Systems*, vol. 19, no. 8, pp. 2830–2841, 2021.

[69] R. Lal, W. Huang, and Z. Li, "An application of the ensemble Kalman filter in epidemiological modelling," *Public Library of Science One*, vol. 16, no. 8, Article ID e0256227, 2021.

[70] C. Drovandi, R. G. Everitt, A. Golightly, and D. Prangle, "Ensemble MCMC: accelerating pseudo-marginal MCMC for state space models using the ensemble Kalman filter," *Bayesian Analysis*, vol. 17, no. 1, pp. 223–260, 2022.

[71] J. Arróspide and L. Salgado, "On-road visual vehicle tracking using Markov chain Monte Carlo particle filtering with metropolis sampling," *International Journal of Automotive Technology*, vol. 13, no. 6, pp. 955–961, 2012.

[72] J. Y. Ching and Y. C. Chen, "Transitional Markov chain Monte Carlo method for Bayesian model updating, model class selection, and model averaging," *Journal of Engineering Mechanics*, vol. 133, no. 7, pp. 816–832, 2007.

[73] E. Cai, Y. Zhang, X. Ji et al., "Estimating small structural motions from multi-view video measurement," *Engineering Structures*, vol. 275, Article ID 115259, 2023.